Shock propagation in narrow channels

M. Sun, T. Ogawa, and K. Takayama

Shock Wave Research Center, Institute of Fluid Science, Tohoku University, Katahira 2-1-1, Aoba, Sendai, 980-8577, Japan

1 Introduction

Recent medical and industrial applications of shock waves necessitate a better understanding of shock wave motion at low Reynolds numbers, for example, shock motion in very small tubes ($r < 1mm$) and micron size particles moving at a supersonic speed. The techniques for diagnosis and visualization of such flows are extremely limited due to the small scale of the problems. Numerical simulation might become an more efficient and economic way to analyze such flows. However, numerical modeling and solution scheme for viscosity-dominated time-dependent compressible flows face some difficulties. Some discrepancies have been found between numerical solutions of the Navier-Stokes equations and experimental data obtained in shock tubes [1,2]. It was noticed that even using fine grid cells of a few micrometers the solution of the Navier-Stokes equations still mismatches experimental data of shock wave reflection transition over a wedge[3]. More experiment data are required to choose or even to establish reliable numerical models and schemes for these problems. The propagation of shock waves in narrow channels is believed to be a suitable test case that has a few merits in providing information on the viscosity-dominated compressible flows. Its setup for both experiment and for numerical simulation is simple. Two-dimensionality of the flow in channels enables precise measurement and visualization in experiment, and the length and height of channels may be adjusted to meet the conventional diagnosis techniques; it also allows accurate discretization of numerical models using fine cells.

Despite the behavior of shock wave motion in large shock tubes at relatively high Reynolds numbers were extensively investigated in 1950s and 60s [4–6], little work has been done for low Reynolds number flows, especially in small scales. Shock wave motion at low Reynolds numbers is governed by viscosity as well as convection. A one-dimensional model with the Reynolds analogy for heat and momentum transfer could be applied to the phenomenon of shock and detonation attenuation in narrow channels[7]. Many other models have also been proposed [6,8,9]. However, as pointed out by Duff [10], the solution of this problem requires the finding of a two-dimensional unsteady solution of the Navier-Stokes equations. It is doubtful that the inclusion of transport phenomena as perturbations to a simple shock-tube flow would be adequate for a reliable flow description.

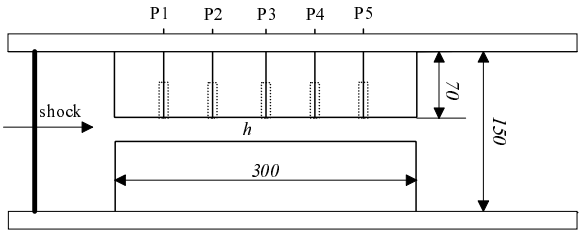

Fig. 1. Experimental setup

In the case of shock wave propagation in a channel, the Reynolds number may be defined as

$$Re = \frac{\rho U h}{\mu}, \tag{1}$$

where ρ, U and μ are density, velocity and viscosity coefficient behind an incident shock wave, and h is the height of the channel. This definition gives a measure of viscosity effects on shock propagation in channels with various heights at different initial pressures. Low initial density or pressure under a constant temperature plays the same role as a small tube does if the product of ρ and h is kept the same. In this sense, the present work is closely related to experiments and analysis for low pressure flows [8–10].

In this work, the propagation of shock waves in channels was investigated experimentally and numerically. Experiments were conducted for five channels with the height ranging from $1mm$ to $16mm$ at initial pressures $10^5 Pa$. By keeping the incident shock Mach number unchanged but setting initial pressure be $10^4 Pa$, we could further scale down the height of channel to $0.1mm$ equivalently. Channel flows were visualized by the double exposure holographic interferometry and pressures at five stations were also measured. The numerical solutions agree with experiment data within the error of measurement. More precise measurement and visualization will be performed to be able to distinguish the difference between experiment and numerical simulation.

2 Experiment and numerical simulation

Experiments were conducted using a $60mm \times 150mm$ diaphragmless shock tube in the Shock Wave Research Center, Institute of Fluid Science, Tohoku University [11]. The scatter of shock wave Mach numbers was found to be within $\pm 0.25\%$ for more than 500 runs. A schematic setup of the channel section is shown in Fig. 1. Two pieces of $300mm$ long steal block were fixed on the shock tube. The upper one was $70mm$ high, inside which five pressure transducers were set at every $50mm$ distance. The height of the narrow channel formed between two blocks, h, was determined by choosing an appropriate height of the lower

(a) (b)

Fig. 2. Example of solution-adaptive grids in a $2mm$ high channel: (a) $p_0 = 10^5 Pa$; (b) $p_0 = 10^4 Pa$

piece. Five channels with the height of $1mm$, $2mm$, $4mm$, $8mm$ and $16mm$ were tested at room temperature $297 \pm 2K$. The channel walls were finely polished. All experiments were conducted only for incident shock Mach number $M_s = 1.2$ in air but under two initial pressures, $10^5 Pa$ and $10^4 Pa$. It should be noted that is not easy to generate a shock wave with $M_s = 1.2$ if the initial pressure is set to $10^4 Pa$ in a convectional shock tube. Channel flows were visualized by the double explosion holographic interferometry that has been a routine technique in the Center for many years. The laminar Navier-Stokes equations were used to model shock motion and its associated flows. The coefficients of viscosity and heat-conductivity were functions of temperature, and assumed to follow Sutherland's formula. The channel walls were set to be isothermal, and its temperature was taken as that in front of the incident shock wave. Wall roughness and rarefied gas effects were not taken into account. The MUSCL-Hancock scheme (see [12], for formulations on structured grids) was applied to unstructured grids. The scheme is second order accurate in both time and space. The gradients or slopes of primitive values at cells were calculated by the least square method. The MINMOD limiter was used in the present computations. A HLLC approximate Riemann solver [12] was chosen to determine the flux at interface because its simplicity and its ability to resolve contact surface. Viscous and heat transfer terms were discretized using a central scheme. A solution-adaptive technique using quadrilateral grids [13] was used to enhance the resolution of shock wave and boundary layer regions. Grid cells were refined in regions with large density and vorticity variations. Five-level refinement was employed in all computations, and the minimum cell sizes were approximately $60\mu m$ along the tube direction and $20\mu m$ normal to it. An example of adaptive grids and numerical density close to the channel entrance is shown in Fig. 2.

3 Results and discussion

3.1 Flow visualization

Shock propagation in $8mm$ and $16mm$ high channels are shown in Fig. 3 and Fig. 4 respectively. The time when the incident shock wave exactly arrived at the entrance is set to zero. Since the incident shock wave moved from a large shock

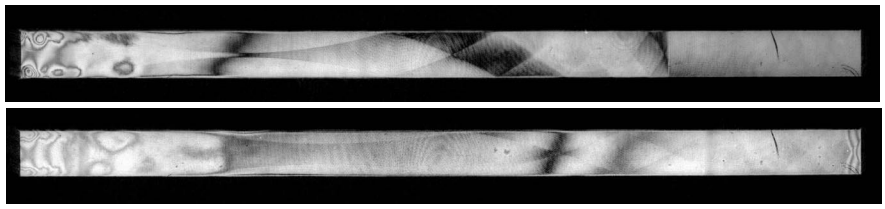

Fig. 3. Shock propagation in a channel, $h = 16mm$, $p_0 = 10^5 Pa$, $M_s = 1.2$: (a) $t = 500\mu s$; $t = 700\mu s$.

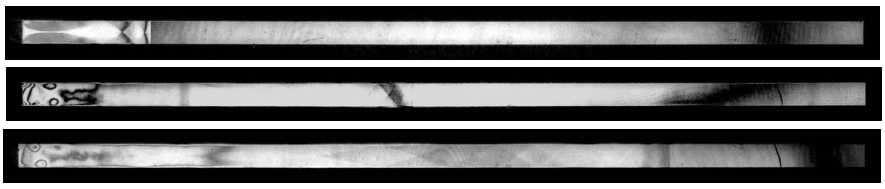

Fig. 4. Shock propagation in a channel, $h = 8mm$, $p_0 = 10^5 Pa$, $M_s = 1.2$: (a) $t = 100\mu s$; $t = 300\mu s$; $t = 500\mu s$.

tube to the narrow channel as shown in Fig. 1, the transmitted shock wave was accelerated by compression and reflected shock waves behind. Numerous weak shock waves are visible in the $16mm$ high channel even after the transmitted shock moved out of observation window as shown in Fig. 3b. These waves are hardly observable after $500\mu s$ in the $8mm$ high channel as shown in Fig. 4c. It is not easy to analyze the effect of viscosity on shock propagation before the disturbances disappear because both of them affect the propagation of shock wave. We found numerical solution of the Euler equations agrees very well with the flow in the $16mm$ case except in the vortex region close to the entrance. This suggests that viscous effects on shock attenuation are negligibly small in wide channels as one may expected.

A uneven boundary layer is developed on each wall of the $4mm$ high channel as shown in Fig. 5. They are nearly symmetric on the upper and lower walls. Reflecting waves form a cell structure between two boundary layers. There is an interesting bump in the boundary layer pointed by an arrow. The bump structure was also observed in other experiments. It is seen from Figs. 5b and c that the bump moved downstream. The mechanism of its development and evolution is not clarified yet. It might be initiated from the corner of the entrance.

The boundary layers on the upper and the lower walls start to merge together in the $2mm$ high channel. The shock wave is significantly attenuated due to skin friction and heat conduction through channel walls. Comparing the locations of shock wave in $1mm$ and $2mm$ high channels shown in Figs. 6a and b, one may find the shock in $1mm$ case is delayed comparing with the $2mm$ case. The location of shock wave in the present channel design is influenced mainly by two factors. One factor is compression waves that accelerate a shock wave, which can be sufficiently described by the Euler equations, and the other is

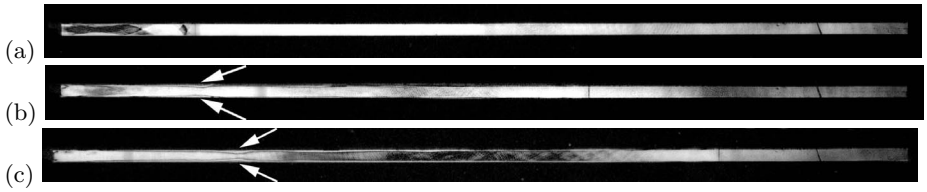

Fig. 5. Shock propagation in a channel, $h = 4mm$, $p_0 = 10^5 Pa$, $M_s = 1.2$: (a) $t = 100\mu s$; $t = 400\mu s$; $t = 500\mu s$.

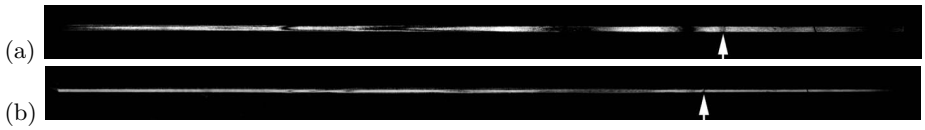

Fig. 6. Shock propagation in a channel, $p_0 = 10^5 Pa$, $M_s = 1.2$, $t = 500\mu s$: (a) $h = 2mm$; (b) $h = 1mm$

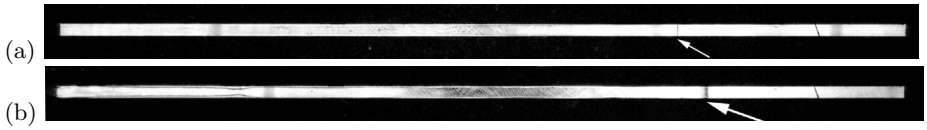

Fig. 7. Shock propagation in a channel, $h = 4mm$, $M_s = 1.2$, $t = 500\mu s$: (a) $p_0 = 10^4 Pa$; (b) $p_0 = 10^5 Pa$

surface friction and heat conduction at wall. This will be further discussed from pressure data in the next subsection. If initial pressure is decreased while keeping the incident shock Mach number constant, the influence of the compression waves should be unchanged. Therefore the difference between experiments at two initial pressures is mainly due to the effects of viscosity. Fig. 6 gives two photos taken at $p_0 = 10^4 Pa$ and $10^5 Pa$ respectively in the $4mm$ channel. The shock wave at the low pressure is about $1.5cm$ behind that in the high pressure after $500\mu s$ propagation in the channel.

3.2 Pressure measurement

Five pressure transducers were installed on the upper wall of the channels at every $50mm$ from the entrance, as shown in Fig. 1. The pressure histories are almost the same for the channel height over $4mm$ at pressure of $10^5 Pa$. Fig. 8 shows four sets of pressure histories. For the $4mm$ channel, it is seen that the pressure drops at the low pressure case faster than it does at the high pressure by comparing Figs. 8a and b. The pressure drops dramatically faster at narrower channels and at the low pressure as shown in Figs. 8c and d. In the low Reynolds cases, the shock wave is not a simple step wave, but followed by a continuous increase in pressure. The numerical results, shown in dashed lines, agree with the experimental pressures in general.

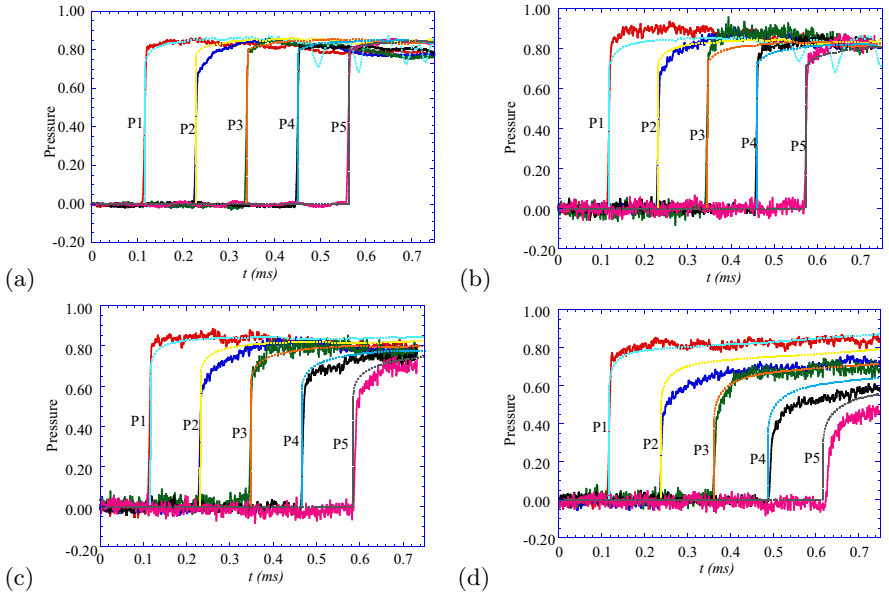

Fig. 8. Pressure histories at five stations along the upper wall, dashed lines are numerical results: (a) $p_0 = 10^5 Pa$, $h = 4mm$; (b) $p_0 = 10^4 Pa$, $h = 4mm$; (c) $p_0 = 10^4 Pa$, $h = 2mm$; (d) $p_0 = 10^4 Pa$, $h = 1mm$.

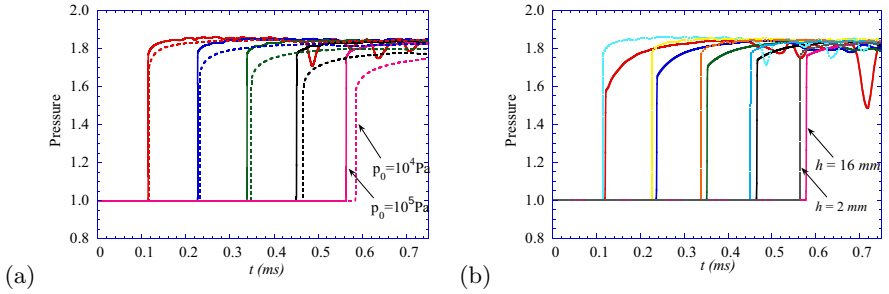

Fig. 9. (a) pressure histories in $h = 2mm$ channel flows at $p_0 = 10^5 Pa$ and $10^4 Pa$; (b) pressure histories in channel flows with $h = 2mm$ and $16mm$ at $p_0 = 10^5 Pa$

Fig. 9a compares pressures in the $2mm$ high channel at the two initial pressures. It is seen that pressure values immediately behind the shock wave at all stations are below for the low initial pressure. Fig. 9b shows pressure histories in $2mm$ and $16mm$ channels. It is seen that the shock in the narrower channel is moving faster although the Reynolds number is low. Because it takes shorter distance for compression waves behind to catch up with shock front in a narrow channel, the shock wave propagates at its maximum speed for a longer distance. This suggests that changing initial pressure is a better way to reduce the Reynolds number than decreasing the channel height.

4 Summary

The propagation of a shock wave in a few narrow channels has been investigated experimentally and numerically for incident shock Mach number $M_s = 1.2$. Viscous effects in channels the height of which is below $4mm$ become noticeable even at atmospheric pressure. It is found that shock wave propagates slower at low pressures in a narrow channel, but it may propagate faster than in a wide channel because the compression waves initiated from the entrance of a channel strengthen the shock wave. The present numerical results agree with experiment in general. The accuracy of present experiments is still not high enough to validate numerical models and solution schemes. To enhance the accuracy, flow visualization will be focused on a local region instead of the whole test section, and more sensitive and precise pressure transducers for measuring weak shock wave at low initial pressures are necessary.

References

1. M. Sun, K. Takayama (2001) Some discrepancies between CFD and shock tube experiments, 14th International Mach Reflection Symposium, Japan
2. T. Saito, K. Takayama (1999) Numerical simulations of nozzle starting proces, *Shock Waves*, v9, pp. 73-79
3. L.F. Henderson, K. Takayama, W.Y. Crutchfield and S. Itabashi (2001) The persistence of regular reflection during strong shock diffraction over rigid ramps, *J. Fluid Mech.*, **431**, pp. 273-296
4. Emrich RJ, Curtis CW (1953) Attenuation in the shock tube, *J. of Applied Physics*, V24, pp.360-363.
5. Glass II, Sisilian (1991) Nonstationary flows and shock waves, Oxford Science Publications.
6. Hollyer RN (1956) Attenuation in the shock tube: I. Laminar flow, *J. of Applied Physics*, V27, pp.254-261.
7. Thomas GO, Brown CJ, Teodorczyk A (2000) Shock and detonation attenuation in narrow channels, preprint for *Experiments in Fluids*.
8. Mirels H (1963) Test time in low-pressure shock tubes, *Physics of Fluids*, V6, pp. 1201-1214.
9. Roshko A (1960) On flow duration in low-pressure shock tubes, *Physics of Fluids*, V3, pp. 835-842.
10. Duff RE (1959) Shock-tube performance at low initial pressure, *Physics of Fluids*, V2, pp. 207-216.
11. Yang JM, Takayama K (1994) Reflection and diffraction of shock waves generated by a diaphragmless shock tube. Proc. 3rd Asian Symp. on Flow Visualization: pp. 259-264.
12. Toro EF (1999) Riemann solvers and numerical methods for fluid dynamics, 2nd edition, Springer.
13. Sun M, Takayama K (1999) Conservative smoothing on an adaptive quadrilateral grid. *J. Comp. Phys*, V150, pp. 143-180.